Asian Journal of Chemistry; Vol. 37, No. 7 (2025), 1636-1640

ASIAN JOURNAL OF CHEMISTRY

https://doi.org/10.14233/ajchem.2025.33868

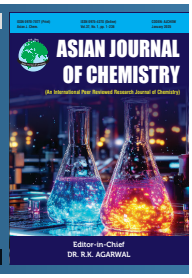

Iron Oxide Nanoparticles as an Efficient Catalyst for Azide-Alkyne Cycloaddition Reaction

MEENA B. LANDE[1,2], MAHESH S. JANGALE[2], SURESH T. GAIKWAD[1] and ANJALI S. RAJBHOJ[1,*]

[1]Department of Chemistry, Dr. Babasaheb Ambedkar Marathwada University, Chhatrapati Sambhajinagar-431004, India
[2]Department of Chemistry, Mula Education Society's Arts, Commerce and Science College, Sonai-414105, India

*Corresponding author: E-mail: anjali.rajbhoj@gmail.com

Received: 12 April 2025; *Accepted*: 2 June 2025; *Published online*: 30 June 2025; AJC-22037

The current work focused on the synthesis of iron oxide nanoparticles by electrochemical method and its application in sustainable and eco-friendly copper-free method for the azide–alkyne cycloaddition reactions using a mild-conditions. The electrochemical reduction method was used to synthesize the iron oxide nanoparticles (IONPs) by optimizing the current density of 10 mA/cm^2 and tetrapropylammonium bromide as a structure-directing agent in an organic medium. A conventional electrolysis cell was used to generate nanoparticles, with a readily available iron metal sheet acts as an anode and a platinum sheet served as a cathode. The synthesized iron oxide nanoparticles were characterized using FTIR, XRD, SEM and energy dispersive X-ray analysis techniques. The reaction is regioselective as Huisgen 1,3-dipolar cycloaddition reaction where 1,4-disubstituted 1,2,3-triazole formed as product. IONPs could be magnetically collected and also reused without any significant loss of its catalytic activity. The synthesized 1,2,3-triazole products were characterized by FTIR, ^{1}H NMR and ^{13}C NMR.

Keywords: Cycloaddition reaction, Electrochemical reduction method, Iron oxide nanoparticles, Tetrapropylammonium bromide.

INTRODUCTION

Iron, the fourth most abundant element in the Earth's crust and the most common transition metal, serves as the structural foundation for our current infrastructure. The three most likely forms of iron oxides in nature are hematite (α-Fe_2O_3), maghemite (γ-Fe_2O_3) and magnesia (Fe_3O_4) [1]. Due to its structural properties, it can be used in a variety of ways in fields such as biology, magneto-optical as well as catalysis, magnetic recording medium, magnetic resonance imaging and drug administration.

A several different methods have been investigated for the synthesis of iron oxide nanoparticles (IONPs) including sol-gel process [2], W/O microemulsion techniques [3], thermal decomposition [4], mechanochemical method [5], hydrothermal synthesis [6], laser pyrolysis [7], flow injection synthesis [8], flame spray pyrolysis [9], coprecipitation method [10] and ball-milling [11]. These methods ultimately make the process more difficult due to high reaction time and toxic chemicals. The electrochemical procedure has several advantages over other synthesis techniques, such as a high yield, no byproducts, simple nanoparticle isolation, flexibility in ligand selection and control over particle size through current density control [12,13]. The IONPs that would synthesized from this method would help to produce a somewhat stronger responsiveness towards catalytic activity. Electrochemical reduction processes can benefit greatly from the catalytic activity of nanoparticles, which are used in both academia and industry.

A variety of biological actions including antimicrobial [14,15], anti-HIV-type I protease [16], anti-adrenergic receptor agonists [17], anti-allergic and hyperglycemic, anticancer, anti-parasitic, antimalarial, antidiabetic, anti-inflammatory, antiviral, *etc*. [18] are exhibited by compounds with a 1,2,3-triazoles. The copper-catalyzed Huisgen-type alkyne-azide cycloaddition (CuAAC) is the most widely used "click" reaction for adding 1,2,3-triazole groups to organic molecules [19]. Its range of applications and fidelity have been demonstrated by its use in numerous organic synthesis, materials science, polymer science and bioconjugates [20]. Numerous Cu(I) and Cu-based NPs have been used to catalyze Huisgen 1,3-dipolar cycloaddition reactions of azides [21,22]. Moreover, copper on iron was used in azide-alkyne cycloaddition reactions as a scavenger

This is an open access journal, and articles are distributed under the terms of the Attribution 4.0 International (CC BY 4.0) License. This license lets others distribute, remix, tweak, and build upon your work, even commercially, as long as they credit the author for the original creation. You must give appropriate credit, provide a link to the license, and indicate if changes were made.

and catalyst [23]. The first-row transition metal oxides and sulfides, including manganese and cobalt ferrite ($MnFe_2O_4$, $CoFe_2O_4$), manganese(II) oxide (MnO) and sulfide (α-MnS), catalyzed the cycloaddition between azides and methyl propiolate [24]. This study provides an easy and effective approach for the synthesis of α-Fe_2O_3 nanoparticles by electrochemical reduction method. As a catalyst for the azide-alkyne cycloaddition process, α-Fe_2O_3 nanoparticles were utilized.

EXPERIMENTAL

All compounds were procured from Sigma-Aldrich and possessed a purity of 99.99%. The HPLC grade acetonitrile (ACN), tetrahydrofuran (THF) and tetrapropylammonium bromide salt (TPAB) were purchased from Rankem chemicals and Sigma-Aldrich, respectively. Alfa Aesar supplied the sacrificial anode, which was bought in the form of iron and platinum sheets as an inert cathode with a thickness of 0.5 mm and a purity of 99.99%. Using thin-layer chromatography (TLC), the reactions were monitored on pre-coated silica gel F_{254} plates (Merck, USA).

Synthesis of iron oxide nanoparticles (IONPs): IONPs were synthesized by using electrochemical reduction method [25]. An affordable two electrode setup with a 25-30 mL electrolyte solution was used in the procedure. Utilizing both bulk metal oxidation and metal ion reduction to generate size-selective tetrapropylammonium bromide stabilized metal nanoparticles. In this experiment, a platinum sheet (1 cm × 1 cm) as cathode and iron metal sheet (1 × 1 cm) as anode were used. A 0.01 M solution of tetrapropylammonium bromide salt (TPAB) prepared in ACN/THF (4:1) was served as supporting electrolyte and these two electrodes were mounted parallel to one another and separated by 1 cm in the solution. After that, a current of 10 mA/cm^2 was applied for 2 h to complete the electrolysis process. Following electrolysis, these nanoparticles allowed to settle for 1 day. Decanting the solid sample allowed it to be removed from the solution and then being thoroughly cleaned with THF three or four times. Once cleaned, the samples were vacuum-dried in desiccators, heated to 600 ºC for 2 h [26] and then used for characterization.

Characterization techniques: The synthesized IONPs was structurally studied using FTIR, XRD and SEM-EDS methods. After mixing the resulting solid nanoclusters with KBr, the JASCO FTIR 8400 Spectrophotometer was used to record FTIR spectra in the 4000-400 cm^{-1} range. The powdered X-ray diffraction patterns were obtained on the Rigaku X-ray diffractometer (Ultima IV) using Cu*K*α radiation (λ = 1.54 Å). The morphology of the synthesized nanoparticles was investigated using a scanning electron microscope (JEOL 6390LA). The existence and elemental makeup of IONPs were examined using an energy dispersive spectrophotometer (EDS). ^{1}H NMR and ^{13}C NMR spectra were recorded on a BRUKER AVANCE III HD NMR 500 MHz spectrometer.

General procedure for azide-alkyne cycloaddition reactions

General procedure for synthesis of 1,4-disubstituted 1,2,3-triazole derivatives: 1-(4-(Prop-2-ynyloxy)phenyl)-ethanone (0.01 mol) and aryl azide (0.012 mol) dissolved in 10 mL solvent. Sodium ascorbate and 5-10 wt.% IONPs were added to this and thoroughly mixed. The reaction mixture was heated about 3 to 12 h and the completion of the reaction was assessed using TLC (25% ethyl acetate: *n*-hexane). After adding the reaction mixture to ice-cold water, the solid product was separated and filtered before being cleaned with cold water (**Scheme-I**). The catalyst was then recovered and recycled.

1-(4-((1-(4-Trifluromethylphenyl)-1*H*-1,2,3-triazol-4-yl)methoxy)phenyl)ethanone (3a): Yellow colour powder. Yield: 0.110 g, 80%. m.p.: 168-170 ºC (decomp.), IR (KBr, ν_{max}, cm^{-1}): 1698, 1629, 1228, (C=O, C=N, C-O); ^{1}H NMR (500 MHz, DMSO-d_6) δ ppm: 8.11 (s, 1H), 7.96 (dd, *J* = 2 & 8 Hz, 2H), 7.53 (m, 3H), 7.18 (dt, *J* = 2 & 8 Hz, 1H), 7.07 (dd, *J* = 1.5 & 7 Hz, 2H), 5.37 (s, 2H), 2.57(s, 3H); ^{13}C NMR (125 MHz, DMSO-d_6) δ ppm: 196.72, 164.33, 161.89, 138.05, 137.95, 131.35, 131.26, 130.97, 130.68, 121.05, 116.04, 115.91, 115.87, 114.48, 108.52, 108.26, 61.97, 26.37.

1-(4-((1-(4-Flurophenyl)-1*H*-1,2,3-triazol-4-yl)methoxy)phenyl)ethanone (3b): White colour powder. Yield, 0.120 g, 73%. m.p.: 144-146 ºC (decomp.), IR (KBr, ν_{max}, cm^{-1}): 1707, 1629, 1228, (C=O, C=N, C-O); ^{1}H NMR (500 MHz, DMSO-d_6) δ ppm: 8.18 (s, 1H), 7.98-7.95 (dt, *J* = 3 & 8 Hz, 2H), 7.92-7.94 (d, *J* = 8 Hz 2H), 7.84-7.82 (d, *J* = 8 Hz, 2H), 7.09-7.07 (d, *J* = 9 Hz, 2H), 5.39 (s, 2H), 2.57(s, 3H); ^{13}C NMR (125 MHz, DMSO-d_6) δ ppm: 196.70, 161.84, 139.26, 131.02, 130.84,

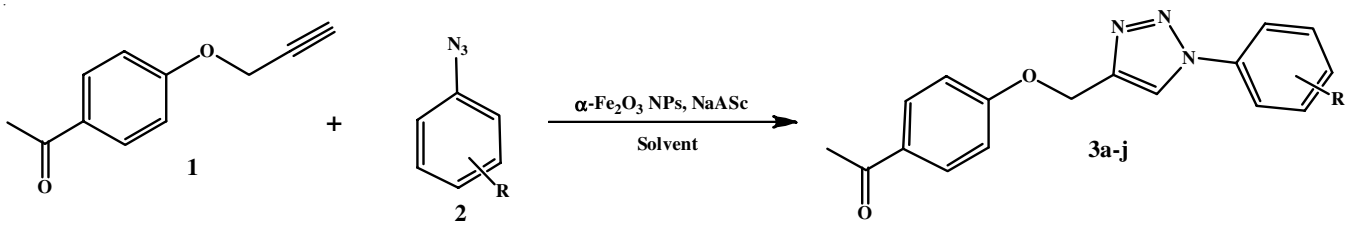

Entry	R	Time (h)	Yield (%)	Entry	R	Time (h)	Yield (%)
3a	4-CF_3	4.0	80	**3f**	2-OCH_3	6.0	68
3b	4-F	3.5	73	**3g**	3-F	5.0	80
3c	3-NO_2	4.0	82	**3h**	4-NO_2	5.0	70
3d	-H	3.0	80	**3i**	3-Cl	7.0	60
3e	4-CH_3	4.0	72	**3j**	2-F	4.5	69

Scheme-I: Synthesis of 1-4 disubstituted 1,2,3-triazole derivatives

130.69, 127.21, 127.17, 124.88, 120.93, 120.54, 114.46, 61.94, 26.37.

1-(4-((1-(3-Nitrophenyl)-1*H*-1,2,3-triazol-4-yl)methoxy)-phenyl)ethanone (3c): Yellow colour powder. Yield, 0.1 g, 82%. m.p.: 156-158 ºC (decomp.), IR (KBr, ν_{max}, cm^{-1}): 1714, 1629, 1228, (C=O, C=N, C-O); ^{1}H NMR (500 MHz, DMSO-d_6) δ ppm: 8.63 (t, *J* = 2 Hz, 1H), 8.34 (ddd, *J* = 1, 2& 8 Hz, 1H), 8.3 (s, 1H), 8.22 (ddd, *J* = 1, 2 & 8 Hz, 1H), 7.97 (d, *J* = 9 Hz, 2H), 7.8 (t, *J* = 8 Hz, 1H), 7.1 (dd, *J* = 2 & 8 Hz, 2H), 5.40 (s, 2H), 2.58 (s, 3H); ^{13}C NMR (125 MHz, DMSO-d_6) δ ppm: 196.72, 164.33, 161.89, 138.05, 137.95, 131.35, 131.26, 130.97, 130.68, 121.05, 116.04, 115.91, 115.87, 114.48, 108.52, 108.26, 61.97, 26.37.

RESULTS AND DISCUSSION

FTIR studies: In Fig. 1, the two distinctive peaks at 430.13 cm^{-1} and 520.78 cm^{-1}, are related to the Fe-O bond. Stretching and vibration modes of the Fe-O bonds are responsible for the bands observed in 650-400 cm^{-1} region. The band at 430.13 cm^{-1} and 520.78 cm^{-1} represent the Fe-O bonds of magnetite nanoparticles and are similar to the results of Basavegowda *et al.* [27]. The tetrahedral site's intrinsic metal stretching vibrations were responsible for the metal-oxygen band at 520.78 cm^{-1}, while Fe-O octahedral site metal stretching was responsible for the metal-oxygen band at 430.13 cm^{-1} [28-30].

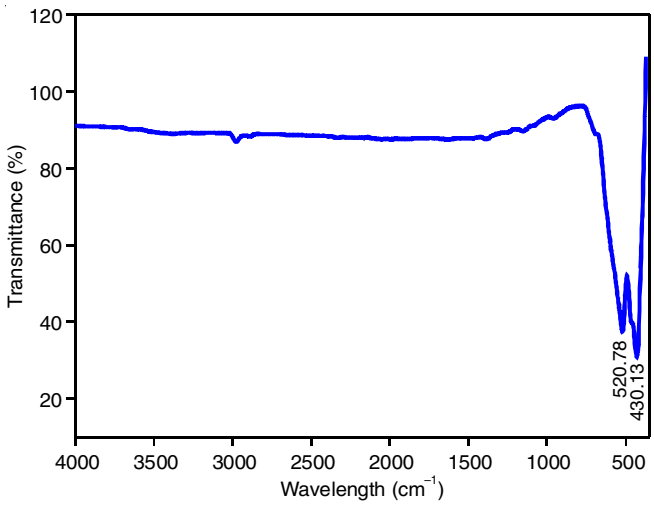

Fig. 1. FT-IR spectra of IONPs

XRD studies: The X-ray diffraction pattern of IONPs that was annealed for 2 h at 600 ºC is shown in Fig. 2. The diffraction planes of the rhombohedral structure of the α-Fe_2O_3 phase are responsible for the composition of its XRD pattern, which consists of several diffraction peaks (JCPDS card No: 79-0007). These peaks correspond to the diffraction planes of the rhombohedral structure of the α-Fe_2O_3 phase and are (012), (104), (110), (113), (024), (116), (018), (214) and (300) [31].

The average crystallite size (D) can be estimated using the Scherrer's equation:

$$D = \frac{k\lambda}{\beta\cos\theta}$$

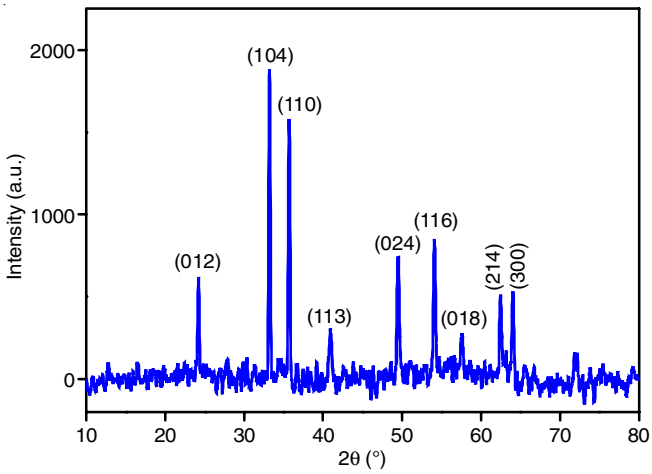

Fig. 2. XRD pattern of IONPs

where D is the average particle size (nm); k is the Scherrer's constant, which typically takes a value of 0.98; λ is the X-ray wavelength; θ is the diffraction angles; β is the Full-width at half maximum (FWHM).

The intensive peaks at (104) was considered for the calculation of the crystallite size. The value of D was about 32 nm. Lassoued *et al*. [32] reported the hematite grain size decreases from 33 to 21 nm when the deposition mechanism change from hydrothermal to precipitation. Mathevula *et al.* [33] has successfully lowered the size of the nanopowder crystallites to 0.94 nm by doping the hematite produced *via* the sol gel method with helium ions. Shariatzadeh *et al.* [34] obtained a crystallite size of 75.4 nm after calcining α-Fe_2O_3 nanopowder for 1 h at 500 ºC, which was generated using a solvothermal process.

SEM studies: The SEM images represent spherical morphology shown in Fig. 3. The nanocrystals formed of IONPs were agglomerated and the agglomeration can be caused due to van der Waals force and magnetic interactions among the particles [2,35].

EDS studies: The EDS spectra in Fig. 4 shows four peaks corresponding to two peaks for Fe and two peaks for oxygen atom. An analysis using energy-dispersive spectroscopy verified the existence of iron oxide. The capping agent responsible for the partial oxidation of the nanoparticles during sample handling owing to ambient oxygen is the source of the oxygen component. The content of iron and oxygen atoms was determined to be 77.85% and 22.15%, respectively, which clearly confirmed the formation of pure iron oxide nanoparticles.

Catalytic activity: Reaction condition optimization involved the systematic exploration of parameters using 1-(4-(prop-2-ynyloxy)phenyl)ethanone (**2**) and phenyl azide as model reactants refluxed at 70-80 ºC employing α-Fe_2O_3 as catalyst. The synthesis of an 1,4-disubstituted 1,2,3-triazole product was achieved in approximately 3 h, with 10 % of catalyst affording a commendable 80% isolated yield (Table-1, entry 12).

Investigations into catalyst loading were conducted, varying from 5% to 10% and 1 mmol of substrate. Remarkably, employing 5-10% catalyst in DMF, ethanol and isopropanol gives very low yield of product and prolonged time of reaction about 9-12 h heating (Table-1, entries 1 to 3 & 7 to 9). The 5%

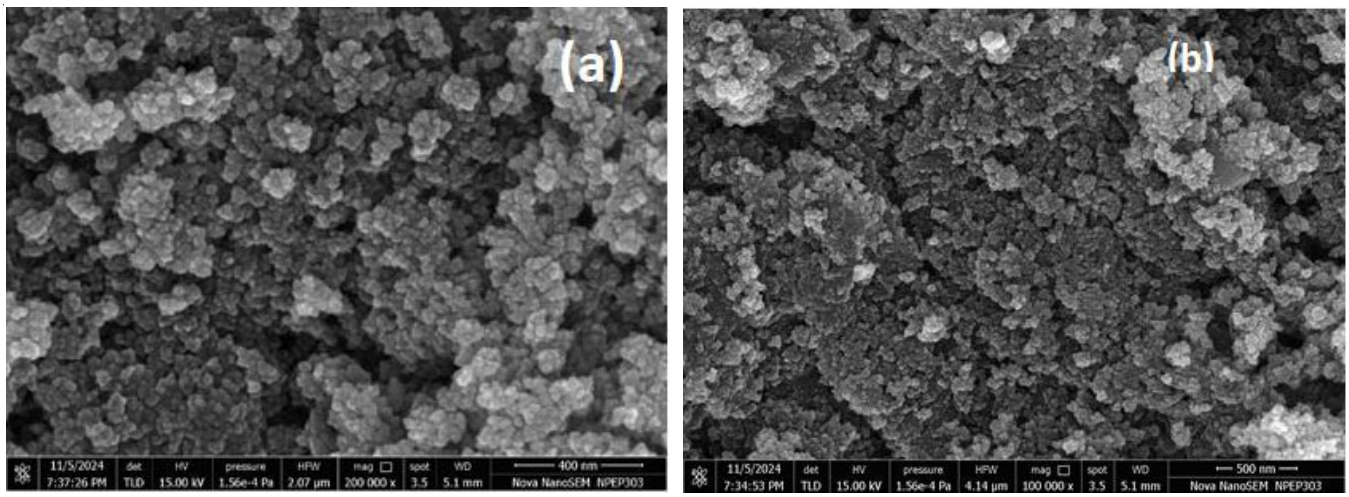

Fig. 3. Scanning electron microscopy (SEM) images of IONPs

TABLE-1
OPTIMIZATION OF THE REACTION CONDITIONS FOR THE PREPARATION OF 1,4-DISUBSTITUTED 1,2,3-TRIAZOLE

Entry	Catalyst (wt.%)	Solvent	Temperature (ºC)	Time (h)	Isolated yield (%)
1	5	DMF	70	12	20
2	5	Ethanol	80	12	10
3	5	Isopropanol	70	10	25
4	5	Isopropanol:water (1:1)	70	7	20
5	5	Isopropanol:water (2:1)	70	5	30
6	5	Isopropanol:water (3:1)	70	4	65
7	10	DMF	70	10	25
8	10	Ethanol	80	11	20
9	10	Isopropanol	70	9	25
10	10	Isopropanol:water (1:1)	70	7	30
11	10	Isopropanol:water (2:1)	70	5	40
12	10	Isopropanol:water (3:1)	70	3	80

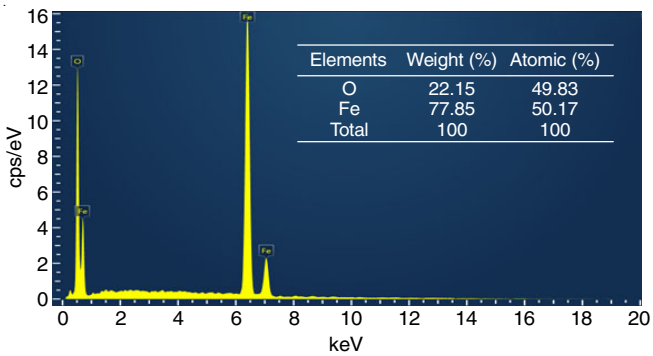

Fig. 4. EDS spectrum of IONPs and composition of elements

of catalyst yielded 65% product in isopropanol & water (3:1) within 4 h (Table-1, entry 6). Interestingly, utilizing 10% of the catalyst yielded a remarkable 80% product yield in isopropanol & water (3:1) within 3 h (Table-1, entry 12). This implies that a higher catalyst concentration corresponds to a faster reaction rate. The concentration of the catalyst directly affects the rate of reaction. The efficiency of reaction was thus decreased due to the decrease in catalyst concentration. Consequently, it was concluded that, under the investigated conditions, the IONPs catalyst operating at a 10% loading demonstrated the best performance in isopropanol & water (3:1) (Table-1, entry 12).

Recovery and reuse of iron oxide nanoparticles catalyst: The two-component synthesis of 1,4-disubstituted 1,2,3-triazole derivatives was selected as the model reaction for examining the catalyst's performance during different recovery and reuse cycles. Notably, despite the small amount of catalyst used (10 wt.%), it was easily separated from the reaction medium, cleaned and reused with the help of a permanent magnet that was placed on the outer wall of reaction flask. This reduced the amount of catalyst that typically loses its properties during filtration processes. After five successive cycles, the catalyst performance for the process as displayed in Fig. 5, with no observable loss of catalytic activity. Little catalyst mass losses throughout the washing process would be the cause of the relatively small activity decrease from the first to the fifth cycle.

Conclusion

An efficient heterogeneous catalyst iron oxide nanoparticles (IONPs) was prepared by electrochemical reduction method. This catalyst is utilized in the the azide-alkyne cycloaddition reactions under mild-conditions by using TPAB stabilizer for azide and alkyne [3+2] cycloaddition. The FTIR analysis of IONPs confirmed that the capping agent had been eliminated during calcinations. The XRD analysis of the IONPs revealed the generation of nanoparticles with a rhombohedral structure and the particle size of 32 nm. The 1,4-disubstituted 1,2,3-tri-

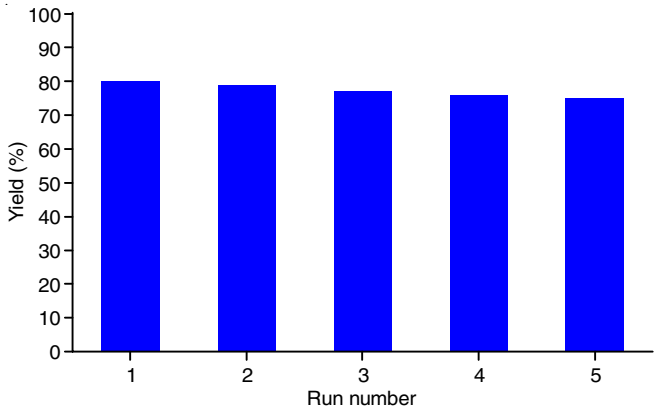

Fig. 5. Recovery and recycling of the iron oxide catalyst

azole regioisomer was synthesized by this heterogeneous approach, which gives a wide scope and excellent results with different azides and alkynes and provides a very high regioselectivity. Furthermore, this heterogeneous IONPs catalyst retains its catalytic activity after at least four reuses and may be magnetically retrieved. The catalyst's facile recoverability and softer reaction conditions for the regioselective synthesis of 1,2,3-triazoles make it suitable for a range of scientific applications.

ACKNOWLEDGEMENTS

The authors are thankful to Department of Chemistry, Dr. Babasaheb Ambedkar Marathwada University, Aurangabad and Principal of Mula Education Society's Arts, Commerce and Science College Sonai, Newasa, Ahilyanagar, India for providing the research studies.

CONFLICT OF INTEREST

The authors declare that there is no conflict of interests regarding the publication of this article.

REFERENCES

1. J. Tucek, L. Machala, S. Ono, A. Namai, M. Yoshikiyo, K. Imoto, H. Tokoro, S.-i. Ohkoshi and R. Zboril, *Sci. Rep.*, **5**, 15091 (2015); https://doi.org/10.1038/srep15091
2. X. Su, S. Chen and Z. Zhou, *Appl. Surf. Sci.*, **258**, 5712 (2012); https://doi.org/10.1016/j.apsusc.2012.02.067
3. K. Wongwailikhit and S. Horwongsakul, *Mater. Lett.*, **65**, 2820 (2011); https://doi.org/10.1016/j.matlet.2011.05.063
4. A. Lassenberger, T.A. Grünewald, P.D.J. van Oostrum, H. Rennhofer, H. Amenitsch, R. Zirbs, H.C. Lichtenegger and E. Reimhult, *Chem. Mater.*, **29**, 4511 (2017); https://doi.org/10.1021/acs.chemmater.7b01207
5. P. A. Calderón Bedoya, P. M. Botta, P. G. Bercoff, and M. A. Fanovich, *J. Alloys Compd.*, **860**, 157892 (2021); https://doi.org/10.1016/j.jallcom.2020.157892
6. P. Bhavani, C.H. Rajababu, M.D. Arif, I.V.S. Reddy and N.R. Reddy, *J. Magn. Magn. Mater.*, **426**, 459 (2017); https://doi.org/10.1016/j.jmmm.2016.09.049
7. A. Criveanu, F. Dumitrache, C. Fleaca, L. Gavrila-Florescu, I. Lungu, I.P. Morjan, V. Socoliuc and G. Prodan, *Appl. Surf. Sci. Adv.*, **15**, 100405 (2023); https://doi.org/10.1016/j.apsadv.2023.100405
8. G. Salazar-Alvarez, M. Muhammed and A.A. Zagorodni, *Chem. Eng. Sci.*, **61**, 4625 (2006); https://doi.org/10.1016/j.ces.2006.02.032
9. R. Tischendorf, M. Simmler, C. Weinberger, M. Bieber, M. Reddemann, F. Fröde, J. Lindner, H. Pitsch, R. Kneer, M. Tiemann, H. Nirschl and H.-J. Schmid, *J. Aerosol Sci.*, **154**, 105722 (2021); https://doi.org/10.1016/j.jaerosci.2020.105722
10. M.O. Besenhard, A.P. LaGrow, A. Hodzic, M. Kriechbaum, G. Bais, L. Panariello, K. Loizou, S. Damilos, M. Margarida Cruz, N.T.K. Thanh and A. Gavriilidis, *Chem. Eng. J.*, **399**, 125740 (2020); https://doi.org/10.1016/j.cej.2020.125740
11. R. Arbain, M. Othman and S. Palaniandy, *Miner. Eng.*, **24**, 1 (2011); https://doi.org/10.1016/j.mineng.2010.08.025
12. O.I. Kuntyi, A.R. Kytsya, I.P. Mertsalo, A.S. Mazur, G.I. Zozula, L.I. Bazylyak and R.V. Topchak, *Colloid Polym. Sci.*, **297**, 689 (2019); https://doi.org/10.1007/s00396-019-04488-4
13. R.A. Khaydarov, R.R. Khaydarov, O. Gapurova, Y. Estrin and T. Scheper, *J. Nanopart. Res.*, **11**, 1193 (2009); https://doi.org/10.1007/s11051-008-9513-x
14. A. Rani, G. Singh, A. Singh, U. Maqbool, G. Kaur and J. Singh, *RSC Adv.*, **10**, 5610 (2020); https://doi.org/10.1039/C9RA09510A
15. M.S. Jangale, N.D. Bhoge, G.M. Sonwane, A.A. Pund and B.K. Magare, *J. Mol. Struct.*, **1308**, 138033 (2024); https://doi.org/10.1016/j.molstruc.2024.138033
16. M.M. Mudgal, N. Birudukota and M.A. Doke, *Int. J. Med. Chem.*, **2018**, 2946730 (2018); https://doi.org/10.1155/2018/2946730
17. L.L. Brockunier, M.R. Candelore, M.A. Cascieri, Y. Liu, L. Tota, M.J. Wyvratt, M.H. Fisher, A.E. Weber and E.R. Parmee, *Bioorg. Med. Chem. Lett.*, **11**, 379 (2001); https://doi.org/10.1016/S0960-894X(00)00669-7
18. K. Bozorov, J. Zhao and H. A. Aisa, *Bioorg. Med. Chem.*, **27**, 3511 (2020); https://doi.org/10.1016/j.bmc.2019.07.005
19. R. Huisgen, *Angew. Chem.*, **13**, 604 (1963); https://doi.org/10.1002/ange.19630751304
20. M. Gauthier and G. Whitton, *Polymers*, **9**, 540 (2017); https://doi.org/10.3390/polym9100540
21. V.V. Rostovtsev, L.G. Green, V.V. Fokin and K.B. Sharpless, *Angew. Chem.*, **114**, 2708 (2002); https://doi.org/10.1002/1521-3757(20020715)114:14<2708::AID-ANGE2708>3.0.CO;2-0
22. F. Alonso, Y. Moglie and G. Radivoy, *Acc. Chem. Res.*, **48**, 2516 (2015); https://doi.org/10.1021/acs.accounts.5b00293
23. M. Chetia, A.A. Ali, D. Bhuyan, L. Saikia and D. Sarma, *New J. Chem.*, **39**, 5902 (2015); https://doi.org/10.1039/C5NJ00754B
24. G. Molteni, A.M. Ferretti, M.I. Trioni, F. Cargnoni and A. Ponti, *New J. Chem.*, **43**, 18049 (2019); https://doi.org/10.1039/C9NJ04690A
25. M.T. Reetz and W. Helbig, *J. Am. Chem. Soc.*, **116**, 7401 (1994); https://doi.org/10.1021/ja00095a051
26. A.A. Agale, S.M. Janjal, S.T. Gaikwad and A.S. Rajbhoj, *J. Cluster Sci.*, **28**, 477 (2017); https://doi.org/10.1007/s10876-016-1118-4
27. N. Basavegowda, K. Mishra and Y.R. Lee, *RSC Adv.*, **4**, 61660 (2014); https://doi.org/10.1039/C4RA11623B
28. Y.P. Yew, K. Shameli, M. Miyake, N.B.B. Ahmad Khairudin, S.E.B. Mohamad, T. Naiki and K.X. Lee, *Arab. J. Chem.*, **13**, 2287 (2020); https://doi.org/10.1016/j.arabjc.2018.04.013
29. M. Mahdavi, M. Ahmad, M. Haron, F. Namvar, B. Nadi, M. Rahman and J. Amin, *Molecules*, **18**, 7533 (2013); https://doi.org/10.3390/molecules18077533
30. A. Demir, R. Topkaya and A. Baykal, *Polyhedron*, **65**, 282 (2013); https://doi.org/10.1016/j.poly.2013.08.041
31. M. Hjiri, *J. Mater. Sci. Mater. Electron.*, **31**, 5025 (2020); https://doi.org/10.1007/s10854-020-03069-4
32. A. Lassoued, M.S. Lassoued, B. Dkhil, S. Ammar and A. Gadri, *Physica E*, **101**, 212 (2018); https://doi.org/10.1016/j.physe.2018.04.009
33. L.E. Mathevula, L.L. Noto, B.M. Mothudi and M.S. Dhlamini, *Physica B*, **535**, 258 (2018); https://doi.org/10.1016/j.physb.2017.07.053
34. S.M.R. Shariatzadeh, M. Salimi, H. Fathinejad and A.H. Joshaghani, *Int. J. Eng.*, **35**, 1186 (2022); https://doi.org/10.5829/IJE.2022.35.06C.10
35. F.N. Sayed and V. Polshettiwar, *Sci. Rep.*, **5**, 9733 (2015); https://doi.org/10.1038/srep09733